Available online at www.sciencedirect.com
ScienceDirect
Acta Materialia 58 (2010) 14–19
Acta MATERIALIA
www.elsevier.com/locate/actamat

Misorientation texture development during grain growth. Part II: Theory

J. Gruber *, A.D. Rollett, G.S. Rohrer

Department of Materials Science and Engineering, Carnegie Mellon University, 5000 Forbes Avenue, Pittsburgh, PA 15213-3890, USA

Received 28 March 2009; received in revised form 15 August 2009; accepted 17 August 2009
Available online 7 October 2009

Abstract

A critical event model for the evolution of number- and area-weighted misorientation distribution functions (MDFs) during grain growth is proposed. Predictions from the model are compared to number- and area-weighted MDFs measured in Monte Carlo simulations with anisotropic interfacial properties and several initial orientation distributions, as well as a dense polycrystalline magnesia sample. The steady-state equation of our model appears to be a good fit to all data. The relation between the grain boundary energy and the normalized average boundary area is discussed in the context of triple junction dynamics.

Keywords: Texture; Grain growth; Anisotropy; Grain boundaries; Simulation

1. Introduction

In a companion paper [1], hereafter referred to as Part I, we examined misorientation texture development during grain growth using Monte Carlo simulations as well as misorientation measurements from polycrystalline magnesia. It is clear from our results with random orientation texture that both area- and number-weighted misorientation distribution functions (MDFs) evolve to approximate steady states that are measurably different from the initial random state. We attempt to provide a quantitative explanation of these observations in the current work. In what follows we will discuss a new model for MDF evolution during grain growth. This model expands upon ideas introduced by the authors elsewhere [2], presenting a more rigorous derivation by removing several nonphysical assumptions used in the previous model.

Because the number of boundaries of any type changes only by discrete topological events in the grain boundary network, our model is based on the relative rates of such critical events. We first discuss the kinds of permissible topological events that can occur during grain growth and then derive a rate equation for the change in number of grain boundaries as a function of boundary type. In this model we assume that the relative grain boundary area, which has an approximately inverse relationship to boundary energy, influences the probability of a grain boundary being eliminated by topological events. Additionally, we assume that the character of new grain boundaries generated by critical events depends on the orientation texture of the microstructure. The combined result is a quantitative relationship between grain boundary energy, orientation texture, and the expected misorientation texture developed during grain growth. Finally, we discuss how this relation might be used to predict misorientation texture in real materials, and also solve the inverse problem, i.e. determining grain boundary energy anisotropy using misorientation texture data.

2. Model

In the following, we use the word "area" to describe the usual measure of grain boundary size regardless of spatial dimension. We will denote the area- and number-weighted MDFs as $f_A(\theta, t)$ and $f_N(\theta, t)$, respectively. These are both

* Corresponding author. Tel.: +1 412 476 5282.
E-mail address: gruberja@gmail.com (J. Gruber).

1359-6454/$36.00
doi:10.1016/j.actamat.2009.08.032

assumed to be explicit functions of the boundary type, parameterized by θ, and time t. Many other quantities, such as the area or number of boundaries, can be measured for a particular boundary type or for the entire system. To avoid introducing an excess of variables, we will always write system total functions with only a time argument. Thus the total area and number of grain boundaries in the system will be given by $A(t)$ and $N(t)$, while the total area and number of boundaries of a particular type will be $A(\theta,t)$ and $N(\theta,t)$. Likewise, the average boundary area in the system will be $\langle A\rangle(t)$, and the average area for boundary type θ is $\langle A\rangle(\theta,t)$. Note that the following relations hold, by definition:

$$\langle A\rangle(t) = \frac{A(t)}{N(t)} \tag{1}$$

$$\langle A\rangle(\theta,t) = \frac{A(\theta,t)}{N(\theta,t)} = \frac{f_A(\theta,t)A(t)}{f_N(\theta,t)N(t)} \tag{2}$$

The quotient $\langle A\rangle(\theta,t)/\langle A\rangle(t)$ represents a dimensionless average grain boundary area, and has an important role in the current model. Because of this definition, the problem of predicting $f_A(\theta,t)$ and $f_N(\theta,t)$ can be reinterpreted as a problem of predicting, for example, $\langle A\rangle(\theta,t)/\langle A\rangle(t)$ and $f_N(\theta,t)$. This is the approach taken here, motivated by the fact that we will later approximate $\langle A\rangle(\theta,t)/\langle A\rangle(t)$ as an explicit function of the grain boundary energy.

We focus on describing MDF development in systems with a large number of grains. By large we mean to say that statements such as "the probability of a boundary of type θ being eliminated by grain collapse" are meaningful. We will ignore the possibility of the MDF statistic ever being affected by a small number of grain boundaries in the system, or that the domain size or shape contributes in any way to the average properties of the grain boundary network. Of course the simulations presented here, as well as any experimental study, are subject to such conditions.

2.1. Topological events during grain growth

Any change in the number of grain boundaries in a microstructure is necessarily the result of topological changes in the grain boundary network. We will base our classification scheme of critical events on the work of Fortes and Ferro [3], who have described the possible "unit operations" that may occur during grain growth. These topological events are those that preserve the correct valencies of topological features found in a microstructure. Most importantly, any conceivable change in the topological structure of a grain boundary network can be represented as a combination of such events.

In both two and three dimensions, these events will be described as either collapse events or switching events. Collapse events are associated with the collapse of entire grains and occur when grains with three (two-dimensional, 2D) or four (three-dimensional, 3D) faces shrink to a vertex. Switching events involve grains switching topological classes (number of faces and edges) while remaining in the microstructure. These events occur by edge switching (2D), a face-to-edge switch (3D) or their inverses. Switching events occur in pairs and thus preserve the total number of boundaries in two dimensions, but occur independently in three dimensions. We will call the loss of a boundary by switching elimination, while the introduction of a new boundary in the microstructure will be called generation.

In what follows, the cumulative number of grain boundaries lost by grain collapse will be denoted $N_c(t)$, and the cumulative number eliminated or generated by switching events will be denoted $N_e(t)$ and $N_g(t)$, respectively. Without loss of generality, we set each to zero at $t = 0$.

2.2. Critical event model

Using the above definitions, we can write an exact relation for the change in the number of boundaries of type θ during a time interval dt,

$$\begin{aligned} N(\theta,t+dt) - N(\theta,t) = {} & p_g(\theta,t)[N_g(t+dt) - N_g(t)] \\ & - p_e(\theta,t)[N_e(t+dt) - N_e(t)] \\ & - p_c(\theta,t)[N_c(t+dt) - N_c(t)] \end{aligned} \tag{3}$$

Here, $p_g(\theta,t), p_e(\theta,t)$ and $p_c(\theta,t)$ denote the probabilities that each possible topological event involves a boundary of type θ. The bracketed terms on the right-hand side of Eq. (3) are simply the total numbers of each critical event that occur in this time interval. Dividing by dt and taking the limit as the time interval approaches zero, we have the differential equation

$$\begin{aligned} & N(t)\frac{\partial f_N(\theta,t)}{\partial t} + f_N(\theta,t)\frac{\partial N(t)}{\partial t} \\ & \quad = p_g(\theta,t)\frac{\partial N_g(t)}{\partial t} - p_e(\theta,t)\frac{\partial N_e(t)}{\partial t} - p_c(\theta,t)\frac{\partial N_c(t)}{\partial t} \end{aligned} \tag{4}$$

We now define

$$\begin{aligned} \alpha_g(t) &= \frac{\partial N_g(t)}{\partial N(t)} \\ \alpha_e(t) &= \frac{\partial N_e(t)}{\partial N(t)} \\ \alpha_c(t) &= \frac{\partial N_c(t)}{\partial N(t)} \end{aligned} \tag{5}$$

These functions express the relative rates of each critical event type with respect to the change in the total number of boundaries, and satisfy $\alpha_g(t) - \alpha_e(t) - \alpha_c(t) = 1$. Within a fixed time interval, the number of events of each type are of the same magnitude. Measuring these rates from our simulations, we find that each remains nearly constant, i.e. the rate of each type of topological event scales with the total number of grain boundaries and, similarly, the grain size. For generality, we will continue to assume each is time-dependent; their use here is merely intended to simplify the notation. Substituting the definitions in the previous expression into Eq. (4), we have

$$f_N(\theta,t) + N(t)\frac{\partial f_N(\theta,t)}{\partial N(t)} = \alpha_g(t)p_g(\theta,t) - \alpha_e(t)p_e(\theta,t) - \alpha_c(t)p_c(\theta,t) \quad (6)$$

In the case that the number-weighted MDF reaches a steady state, this reduces to

$$f_N(\theta,t) = \alpha_g(t)p_g(\theta,t) - \alpha_e(t)p_e(\theta,t) - \alpha_c(t)p_c(\theta,t) \quad (7)$$

from which it is clear that the steady-state number-weighted MDF depends on an equilibrium of critical event rates.

Now it remains to determine an adequate form for each probability function. Our first assumption, which is satisfied quite generally by our simulations, is simply

$$p_g(\theta,t) = f_0(\theta,t) \quad (8)$$

where $f_0(\theta,t)$ is the texture-weighted misorientation distribution function (TMDF), as defined in Section 4.4 of Part I. This assumption implies that, when new boundaries are generated, they appear between grains that have a relationship given by the TMDF, but otherwise are not correlated.

Next we assume a functional form for the elimination and collapse events. Both types of event can only eliminate a boundary that already exists in the system. We therefore expect that, when the number of a particular boundary type θ is N and the probability of elimination is P, if the number is increased to cN then its probability of elimination is cP, i.e. $p_e(\theta,t)$ and $p_c(\theta,t)$ should both be first-order homogeneous in $f_N(\theta,t)$. We further assume that these probabilities depend on the dimensionless average areas $\langle A\rangle(\theta,t)/\langle A\rangle(t)$ of boundary types. That the smallest boundaries on a grain are the first to be eliminated by topological switching was postulated decades ago by Smith [5]. The probability of elimination therefore should decrease with increasing average area. Likewise, if boundaries with relatively large areas persist on a grain as it loses faces, they should be the most likely to be eliminated by the grain collapse events. The probability of their elimination by collapse should then increase with increasing average area.

Because the observed values of the dimensionless average areas occur only within a small range of one, we approximate each boundary elimination probability by a series expansion in $\langle A\rangle(\theta,t)/\langle A\rangle(t)$ about one. The probabilities must be invariant with uniform scaling of the domain size, and this is guaranteed by the use of dimensionless quantities. For $p_e(\theta,t)$ we take

$$p_e(\theta,t) = f_N(\theta,t)\sum_{i=0}^{\infty} a_{e,i}[\langle A\rangle(\theta,t)/\langle A\rangle(t) - 1]^i \quad (9)$$

Note that, in isotropic grain growth and more generally, when $\langle A\rangle(\theta,t) = \langle A\rangle(t)$, the above should reduce to $f_N(\theta,t)$, so that $a_{e,0} = 1$. Similarly, for $p_c(\theta,t)$ we take

$$p_c(\theta,t) = f_N(\theta,t)\sum_{i=0}^{\infty} a_{c,i}[\langle A\rangle(\theta,t)/\langle A\rangle(t) - 1]^i \quad (10)$$

and, by the same reasoning, $a_{c,0} = 1$.

2.3. Comparison of critical event model with simulation and experiment

Now we apply our model to the special case of determining the steady-state number- and area-weighted MDFs. After some algebraic manipulations, we have the first-order approximation

$$f_N(\theta,t) = f_0(\theta,t)\left[u(t) + v(t)\frac{\langle A\rangle(\theta,t)}{\langle A\rangle(t)}\right]^{-1} \quad (11)$$

where we have set

$$u(t) = \frac{1 + \alpha_e(t)(1 - a_{e,1}) + \alpha_c(t)(1 - a_{c,1})}{\alpha_g(t)} \quad (12)$$

and

$$v(t) = \frac{\alpha_e(t)a_{e,1} + \alpha_c(t)a_{c,1}}{\alpha_g(t)} \quad (13)$$

To obtain the above expression, the power series for both $p_e(\theta,t)$ and $p_c(\theta,t)$ are truncated after terms of first order. In our simulations we find that $u(t)$ takes values around 2, and $v(t)$ of about $-2/3$, so that in much of the applicable range of $\langle A\rangle(\theta,t)/\langle A\rangle(t)$ the right-hand side of Eq. (11) is linear in $\langle A\rangle(\theta,t)/\langle A\rangle(t)$. Thus, to first order,

$$f_N(\theta,t) \approx f_0(\theta,t)\frac{\langle A\rangle(\theta,t)}{\langle A\rangle(t)} \quad (14)$$

or, in multiples of a random distribution,

$$\lambda_N(\theta,t) \approx \frac{\langle A\rangle(\theta,t)}{\langle A\rangle(t)} \quad (15)$$

The appropriate proportionality constant for both equations can be determined by normalizing Eq. (14).

The local value of the number-weighted MDF is plotted against the right-hand side of Eq. (14) in Fig. 1 for each 3D simulation from Part I at 2000 MCS. As noted in Part I, a steady state had been reached in all simulations between 500 and 1000 MCS. For both 3D and 2D simulations (not shown here), the result is a scatter of points lying close to the line $f(x) = x$. This result confirms the quite general applicability of Eq. (14) in predicting the steady-state number-weighted MDF.

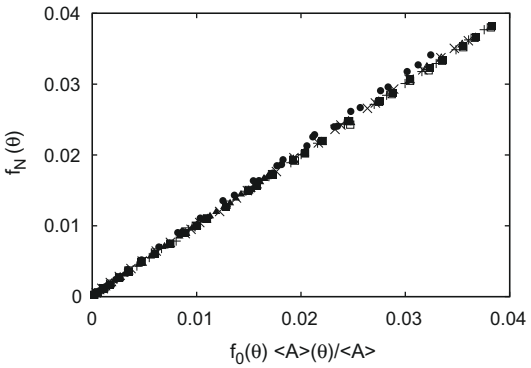

Fig. 1. Scatter plot of the left- and right-hand sides of Eq. (14) for all 3D Monte Carlo simulations with random orientation texture, 2000 MCS.

We note that the initial microstructure in all simulations satisfies Eq. (14) trivially, since we begin with an isotropically grown polycrystal and randomly assigned orientations; however, it is certainly possible to generate a microstructure where the dimensionless average boundary area and the grain boundary number fraction are not related by Eq. (14). For example, starting with a microstructure that satisfies Eq. (14), we can perturb each boundary in a way that perserves the number fraction $f_N(\theta,t)$ but increases or decreases $\langle A\rangle(\theta,t)/\langle A\rangle(t)$ in an arbitrary way. It then appears there is no geometric constraint that suggests Eq. (14) is satisfied a priori. We expect that, in cases where it does not hold, the number-weighted MDF transitions to the steady state according to Eq. (6). However, in our simulations the critical event mechanism appears to operate quickly enough to compensate for changes in the average areas of grain boundaries, leading to the steady-state equation being satisfied at all times. Thus none of the Monte Carlo simulations performed in Part I can be used to test the time dependent part of the critical event model.

Using Eqs. (2) and (14), we can also compute the steady-state area-weighted MDF as

$$f_A(\theta,t) \approx f_0(\theta,t)\left[\frac{\langle A\rangle(\theta,t)}{\langle A\rangle(t)}\right]^2 \tag{16}$$

or, in multiples random,

$$\lambda_A(\theta,t) \approx \left[\frac{\langle A\rangle(\theta,t)}{\langle A\rangle(t)}\right]^2 \tag{17}$$

Again, a suitable proportionality constant can be computed by normalization of Eq. (16). We plot the area-weighted MDF measured in each simulation against the right-hand side of Eq. (16) in Fig. 2. Similar to the result above, we have points lying about a straight line. While the area-weighted MDF now depends on the square of $\langle A\rangle(\theta,t)$, deviations from this line are not significantly larger than those in Fig. 1. Although not shown here, we find that Eq. (16) is approximately satisfied for all simulation times, regardless of whether the area-weighted MDF has reached a steady state.

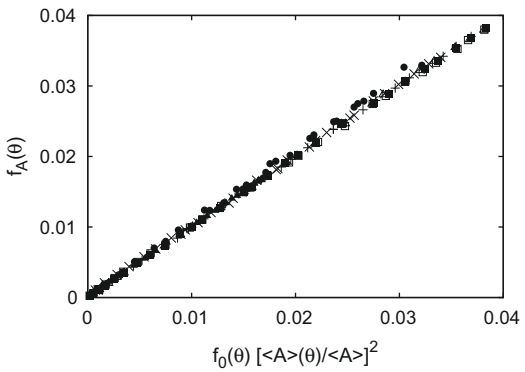

Fig. 2. Scatter plot of left- and right-hand sides of Eq. (16) for all 3D Monte Carlo simulations, 2000 MCS.

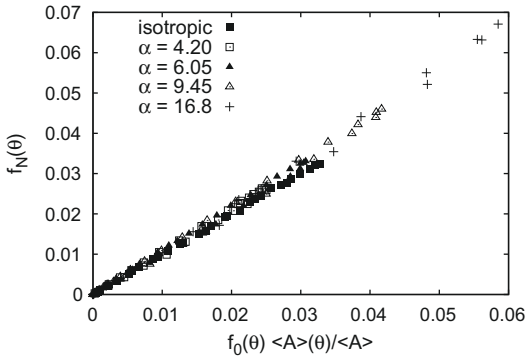

Fig. 3. Scatter plot of left- and right-hand sides of Eq. (14). 3D Monte Carlo simulations with nonrandom orientation texture.

It is possible that the steady-state equation is also satisfied in simulations with nonrandom orientation texture, where $f_0(\theta,t)$ changes with time. In fact, this appears to happen quite generally, as shown in Fig. 3. Clearly, the critical event mechanism occurs on a shorter time scale than the mechanisms controlling average boundary area increases and orientation texture development.

We do not know whether the magnesia sample from Part I has reached a steady-state MDF or orientation texture. However, the results above suggest that Eq. (14) might apply in this case regardless. In fact, we find that the relation is satisfied quite well, as shown in Fig. 4.

2.4. Boundary lengthening model

Aside from the TMDF, the essential input to the critical event model presented above is the average area for each boundary type. A quantitative model for average boundary area has already been presented by Holm et al. [4]. This model introduces the mechanism of boundary lengthening at triple junctions, which has recently been justified experimentally [6]. They consider a 2D geometry where the ends of a grain boundary with energy $\gamma(\theta)$ meet in triple lines with two other boundaries having energy $\gamma_{\max}$, the maximum grain boundary energy in the system, as shown in Fig. 5. To begin, the boundaries are in an isotropic

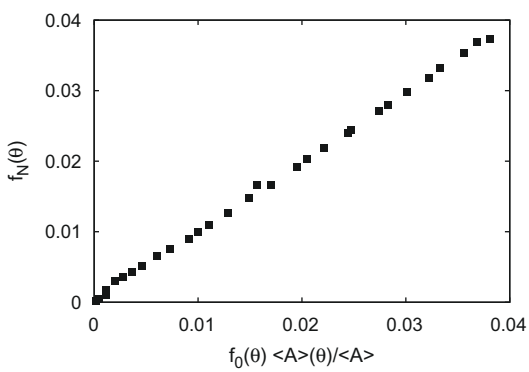

Fig. 4. Scatter plot of left- and right-hand sides of Eq. (14) for polycrystalline magnesia.

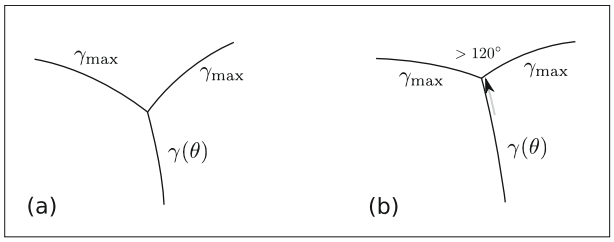

Fig. 5. Schematic of grain boundary-lengthening process. A boundary with energy $\gamma(\theta)$ intersects two boundaries with the maximum grain boundary energy in an isotropic configuration. Boundary lengthening occurs as the boundaries adjust to satisfy mechanical equilibrium at the triple junction.

configuration, i.e. all boundaries have the same length L and every dihedral angle is 120°. Now we let the boundaries relax until the equilibrium triple line geometry is obtained. The boundary with energy $\gamma(\theta)$ now has length $L + \Delta L(\theta)$. Holm et al. used a linear approximation for the boundary lengthening, i.e.

$$\frac{\Delta L}{L} = 1 + \alpha(1 - \gamma(\theta)) \tag{18}$$

where α is a constant fitting parameter. Note that Eq. (18) was derived under the condition that $\gamma_{\max} = 1$. However, we could easily compute the exact lengthening in such a case as [2]

$$\frac{\Delta L}{L} = \frac{1}{2}\left[1 - \frac{\sqrt{3}}{\tan\cos^{-1}\frac{\gamma(\theta)}{2\gamma_{\max}}}\right] \tag{19}$$

This approach does not require a fitting parameter. In both models, the boundary lengthening that occurs for this particular geometry is assumed to be representative of the average boundary lengthening throughout the system. For two dimensions, the increase in boundary area should be proportional to the boundary lengthening given by either Eq. (18) or Eq. (19). Three-dimensional area changes should follow the square of this relation.

Each boundary lengthening model predicts the general trends of average boundary area with energy as measured from our simulations. Fig. 6 shows that the average boundary area is a nonlinear function of energy in both two and three dimensions, especially in the low-energy regime. Eq. (18) does not accurately predict the average boundary areas in regions where the data curves upward, e.g. for the lowest energy grain boundaries, regardless of the chosen fitting parameter. We find that the "exact" lengthening model in Eq. (19) is even less accurate, and in fact exhibits curvature in the opposite direction.

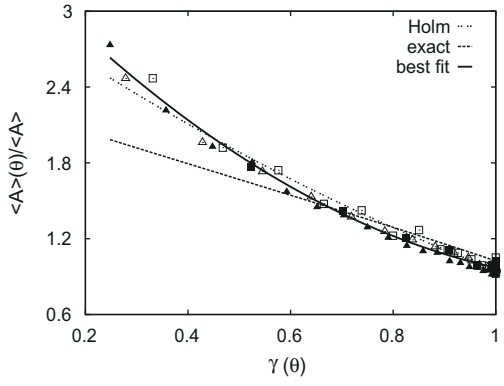

Fig. 6. Scatter plot of grain boundary energy and average boundary area for 3D Monte Carlo simulations. Lines indicate boundary lengthening model predictions and polynomial fit.

Several approximations used in the boundary lengthening model may also contribute to its inaccuracy. First, the topological neighborhood of any grain boundary is certainly more complex than that used, i.e. with every boundary under consideration intersecting only boundaries of the system average energy. A more accurate form of the model might consider the boundary lengthening process of a given boundary type in a number of neighborhoods with boundaries of various energies. Additionally, the three boundaries meeting at a triple junction must satisfy the geometric constraint that $\Delta g_{AB}\Delta g_{BC} = \Delta g_{CA}$ (or any permutation of A, B, and C). For disorientation angles, this implies that $\theta_{AB} \leqslant \theta_{BC} + \theta_{CA}$ (for all permutations). In particular, two low-angle grain boundaries meeting at a triple junction necessarily meet with a third low-angle boundary, while triple junctions with high-angle grain boundaries are not as constrained. This condition implies that, in general, low-angle grain boundaries should not lengthen as much as the boundary-lengthening model predicts. A more refined take on the boundary-lengthening model might take this into account.

While there is qualitative agreement between the boundary-lengthening model and our simulation results, it appears to be quite difficult to derive an accurate quantitative model to predict its resulting effect on a microstructure. However, the relation between grain boundary energy and average area is approximately one to one, and we can fit an empirical formula to it. With a second-order polynomial fit

$$\frac{\langle A\rangle(\theta)}{\langle A\rangle} = a + b\frac{\gamma}{\gamma_{\max}} + c\left(\frac{\gamma}{\gamma_{\max}}\right)^2 \tag{20}$$

we find for two dimensions $a = 2.345, b = -1.592$ and $c = 0.2231$, while for three dimensions $a = 3.610$, $b = -4.369$, and $c = 1.729$. In particular, we can easily use Eq. (20) to approximate any of the steady-state MDFs from simulations with random orientation texture, as shown in Fig. 7. The accuracy of the result is very good, especially for low-angle grain boundaries.

We note that, because each of these functions is invertible within the domain of boundary energies, there is a possibility to use them in the context of deriving energy functions from measured misorientation texture data. For example, we consider the area- and number-weighted MDFs from the polycrystalline magnesia sample from Part I. Fig. 8 shows the results of a fit to $\gamma(\theta)$ using Eq. (20) with the 3D fitting parameters. We see that the majority of the points follow a Read–Shockley-type function with $\theta' = 15°$, as expected. Deviations occur in the low-angle region, where the expected scarcity of low-angle boundaries leads to poor statistics. It must be noted that such a

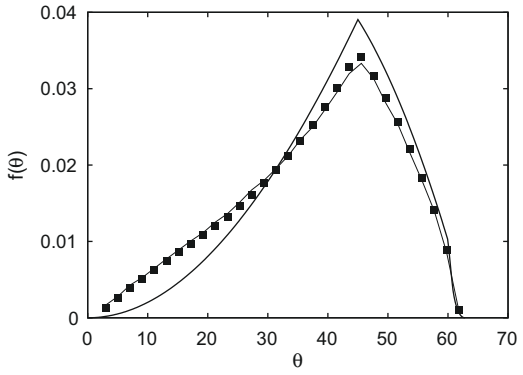

Fig. 7. Steady-state area-weighted MDF computed using the second-order polynomial fit (Eq. (20)), $\gamma_{RS}, \theta' = 45°$. Solid line is the corresponding area-weighted MDF from simulation, 500 MCS.

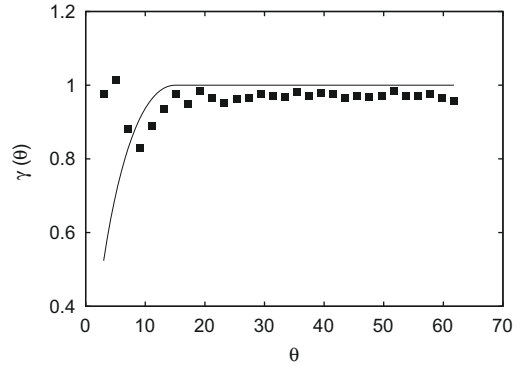

Fig. 8. Energy function derived from MDF measurements of polycrystalline magnesia. Solid line is $\gamma_{RS}, \theta' = 15°$.

derivation is only approximate. In particular, we showed in Part I that boundaries with the same energy may have different average areas, e.g. when the energy is a "step" function. Despite lacking a strict one-to-one correspondence, the method described here should provide a reasonable estimate for the main features of the energy function.

3. Summary

To describe the result of Part I, we have proposed a critical event model for the evolution of number- and area-weighted misorientation distribution functions during grain growth. This model demonstrates the explicit dependence of misorientation texture on grain boundary energy anisotropy and orientation texture through the texture-weighted misorientation distribution function. Predictions from the model are compared to area- and number-weighted MDFs measured in Monte Carlo simulations with random orientation texture and anisotropic interfacial properties. The steady-state equation of our model appears to be a good fit to all data, indicating that the critical event mechanism works on a finer time scale than boundary lengthening or orientation texture development.

Acknowledgements

This work was supported by the MRSEC program of the National Science Foundation under award number DMR-0520425 and by the Computational Materials Science Network program of the Office of Basic Energy Sciences, Department of Energy. J.G. wishes to acknowledge the helpful suggestions provided by E.A. Holm.

References

[1] Gruber J, Miller HM, Hoffmann TD, Rohrer GS, Rollett AD. Acta Mater 2009;57(20):6102–12.
[2] Rohrer GS, Gruber J, Rollett AD. In: Rollett AD, editor. Ceramic transactions. Applications of texture analysis, vol. 201. Hoboken, NJ: John Wiley & Sons; 2009. p. 343–54.
[3] Fortes MA, Ferro AC. Acta Metall 1985;33(9):1697–708.
[4] Holm EA, Hassold GN, Miodownik MA. Acta Mater 2001;49(15):2981–91.
[5] Smith CS. Grain shapes and other applications of topology. In: Metal interfaces. Cleveland, OH: American Society. p. 65–113.
[6] Dillon SJ, Rohrer GS. Acta Mater 2009;57(1):1–7.